J Mater Sci (2007) 42:1501–1511
DOI 10.1007/s10853-006-0753-9

Influence of crystal orientation on the processing of copper single crystals by ECAP

Yukihide Fukuda · Keiichiro Oh-ishi · Minoru Furukawa · Zenji Horita · Terence G. Langdon

Received: 4 April 2006 / Accepted: 2 August 2006 / Published online: 4 January 2007

Abstract Single crystals of high-purity copper, having two different orientations, were pressed through one pass in equal-channel angular pressing (ECAP) at room temperature and then examined using several different analytical techniques. For both orientations, it is shown that elongated arrays of cells or subgrains are formed in the first pass with their long axes aligned parallel to the primary $(\bar{1}1\bar{1})[\bar{1}10]$ slip system. The average width of these subgrains was measured as ~0.2 μm which is similar to the equilibrium grain size reported in polycrystalline Cu after processing by ECAP. These results confirm earlier observations using an aluminum single crystal except only that the subgrain width in copper is significantly smaller. This difference is attributed to the lower stacking-fault energy in copper and the consequent low rate of recovery.

Y. Fukuda · K. Oh-ishi · Z. Horita
Department of Materials Science and Engineering, Faculty of Engineering, Kyushu University, Fukuoka 819-0395, Japan

M. Furukawa (✉)
Department of Technology, Fukuoka University of Education, Munakata, Fukuoka 811–4192, Japan
e-mail: furukawm@fukuoka-edu.ac.jp

T. G. Langdon
Departments of Aerospace & Mechanical Engineering and Materials Science, University of Southern California, Los Angeles, CA 90089-1453, USA

Introduction

Processing through the application of severe plastic deformation (SPD) is now widely accepted as a valuable procedure for achieving substantial grain refinement to the submicrometer or nanometer level [1]. Furthermore, there is an excellent potential for making use of these ultrafine-grained and nanostructured materials in a wide range of commercial applications [2]. Several techniques of SPD processing are available but the most promising appears to be equal-channel angular pressing (ECAP) in which a metal billet, in the form of a rod or bar, is pressed through a die constrained within a channel which is bent through an abrupt angle [3, 4]. There are several advantages of ECAP including the potential for producing bulk solids without the introduction of any residual porosity or contamination, the ease of scaling the process to produce reasonably large samples [5] and the potential for successfully using the same procedure even with difficult-to-work materials such as titanium [6], steel [6] and tungsten [7].

It was recognized in early work that different slip systems may be activated in polycrystalline samples through the simple procedure of rotating the billets between consecutive passes through the ECAP die [3]. These differences are now an important characteristic of the various processing routes that have been developed for the processing of polycrystalline samples by ECAP [8, 9]. However, only very limited attention has been given to the alternative possibility of directly initiating different slip systems in ECAP through the pressing of single crystals having well-defined orientations with respect to the theoretical shear plane within the ECAP die. Very recent reports described a series

of experiments conducted on single crystals of high-purity aluminum in which the single crystals were pressed in ECAP with different initial orientations [10–12]. Accordingly, the present experiments were initiated to extend this approach to single crystals of high-purity copper and to thereby obtain information on the significance of using a face-centered cubic material having a much lower stacking-fault energy and, because of the wide dissociations between the partial dislocations, a relatively low rate of recovery.

Experimental material and procedures

The experiments were conducted using a single crystal rod of high-purity (99.999%) copper with a diameter of 30 mm and a length of 80 mm. The single crystal rod was grown vertically from the melt by the vertical Bridgman method and it was used to supply two ECAP samples having different orientations.

The orientations are depicted schematically in Fig. 1 showing a vertical section through the ECAP die. The two-piece split die was fabricated from SKD11 tool steel in the form of a flat plate and a second plate, shown in Fig. 1, containing a channel bent through an abrupt angle of $\Phi = 90°$. Also present, although not illustrated in Fig. 1 for simplicity in the representation, was an angle of $\Psi = 30°$ representing the outer arc of curvature where the two parts of the channel intersect. The dimensions of this channel were 4×4 mm^2. It is important to note that for internal die angles of $\Phi = 90°$ and $\Psi = 30°$ it can be shown that the strain imposed in a single pass is ~ 1 [13]. Following conventional practice for ECAP [8, 9], an orthogonal coordinate system is defined in which the X or transverse plane lies perpendicular to the flow direction and the Y or flow plane and Z or longitudinal plane lie parallel to the side face and parallel to the top surface at the point of exit from the die, respectively. The theoretical shearing plane, where strain is imposed as the sample passes through the die, lies at 45° to the X direction at the point of intersection of the two parts of the channel.

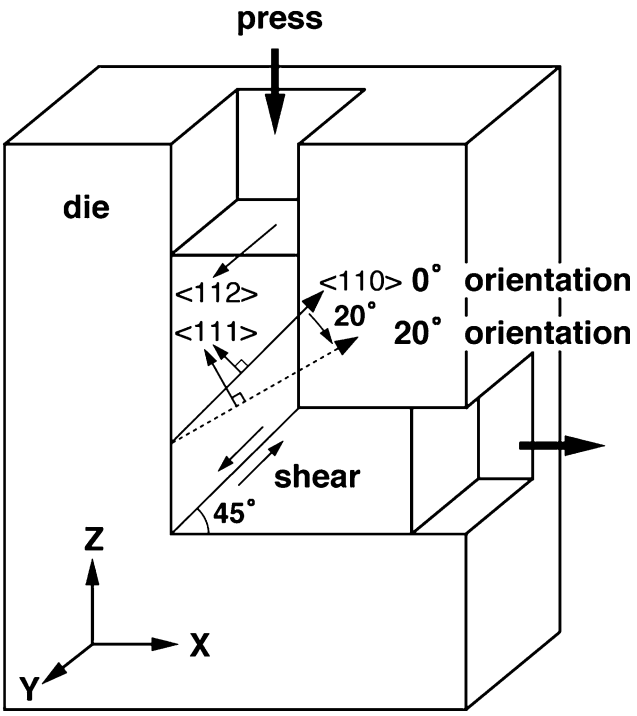

Fig. 1 Schematic illustration of a cross-section through the ECAP die showing the initial 0° and 20° orientations

Two different orientations were used in these experiments. In the first orientation, the {111} slip plane of the single crystal was oriented parallel to the theoretical shear plane within the ECAP die and the ⟨110⟩ slip direction was oriented to lie parallel to the shear direction: this is named the 0° orientation. In the second orientation, a similar crystal was rotated by 20° in a clockwise sense about the Y direction as illustrated in Fig. 1: this is termed the 20° orientation. For both orientations, the Y direction is coincident with the ⟨112⟩ direction as indicated in Fig. 1.

All of the processing by ECAP was conducted at room temperature using single crystals cut in the 0° or 20° orientations with cross-sectional areas of 4×4 mm^2 and lengths of 20 mm. The crystals were pressed using a MoS_2 lubricant and a pressing speed of 18 mm s^{-1}. Prior to pressing, each longitudinal face was carefully polished to a mirror-like finish by grinding on abrasive papers and electropolishing in a solution of 30% HNO_3–70% CH_3OH at a temperature of –20 °C. Following the same procedure adopted earlier for the aluminum single crystals [10–12], each crystal was pressed partially through the die in a single pass and the pressing was terminated when the crystals were in the vicinity of the mid-point of the die. The ECAP die was then opened and the single crystal carefully removed and sectioned longitudinally on the Y plane into two separate and approximately equal pieces. These pieces were used for metallographic observations using optical microscopy (OM), scanning electron microscopy (SEM), orientation imaging microscopy (OIM) and transmission electron microscopy (TEM). Almost all of the observations were performed on the Y plane but for each sample some additional OM observations were undertaken by sectioning to reveal the X plane.

For the observations by OM, the surface was prepared by SiC paper and by alumina paste and then it was electropolished in 30% HNO_3–70% CH_3OH at –20 °C. Etching was performed using a solution of 50 ml distilled water and 5 g of $(NH_4)_2S_2O_8$ at 40 °C. The SEM and OIM were performed using a JEM-5600 scanning electron microscope equipped with an OIM capability. The image area was set at 150×150 μm^2 for the OIM observations and individual measurements were taken in incremental steps of 1.5 μm. The TEM was conducted using an Hitachi H-8100 transmission electron microscope and samples were prepared by punching a disk with a diameter of 3 mm and thickness of ~150 μm and electropolishing in a solution of 20% HNO_3–20% $C_3H_5(OH)_3$–60% CH_3OH at a temperature of –20 °C.

Characteristics of the slip systems in the Cu single crystals

Before examining the experimental results, it is necessary to establish the characteristics of the slip systems in the two Cu single crystals. Figure 2 depicts a schematic illustration of the relationship between the slip direction and the slip plane in the single crystal and the shear direction and shear plane within the ECAP die. Thus, the vertical arrow at upper left denotes the direction of pressing in a vertical sense, F is defined as the force in the shear direction acting on the shear plane with an area of A, and the shear stress, τ, operating on the slip plane in the slip direction is given by the following relationship for each possible slip system:

$$\tau = \left(\frac{F}{A}\right)\cos\theta\cos\lambda \tag{1}$$

where θ is the angle subtended between the two normals to the shear plane and the slip plane and λ is the angle between the shear direction and the slip direction, respectively. In practice, it follows from Eq. 1 that the angular term ($\cos\theta\,\cos\lambda$) represents the shear factor which has values in the range from 0 to 1 and can be calculated individually for each possible slip system.

Figure 3 shows a stereographic projection for the relationship, as viewed in the Y plane, between the 0° orientation and the vertical pressing direction represented by the upper vertical arrow. The 20° orientation is similar to Fig. 3 except only that it is rotated in a clockwise sense by 20° about the mid-point. Using these stereographic projections, the values of the shear factors were estimated for the different possible slip systems and the results are shown in Tables 1 and 2 for the 0° and 20° orientations, respectively. This tabulation incorporates the arc of curvature of Ψ = 30° within the ECAP die, it lists the slip planes and slip directions in the first two columns and the calculated magnitudes of the shear factors are then given in the third, fifth and seventh columns for positions at the

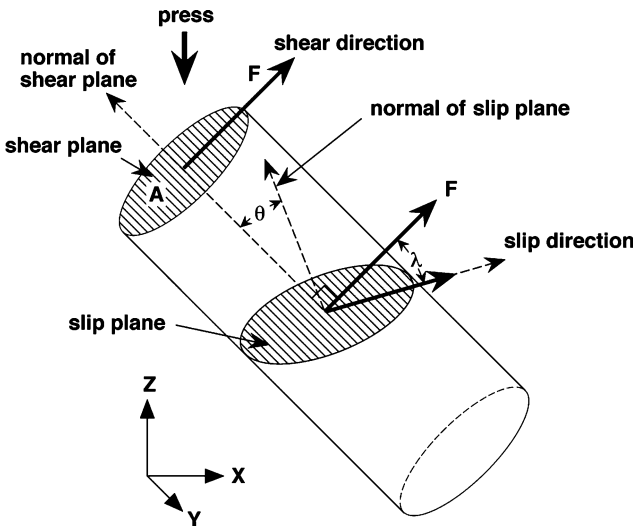

Fig. 2 Schematic illustration of the procedure for estimating the resolved shear stresses associated with different slip systems

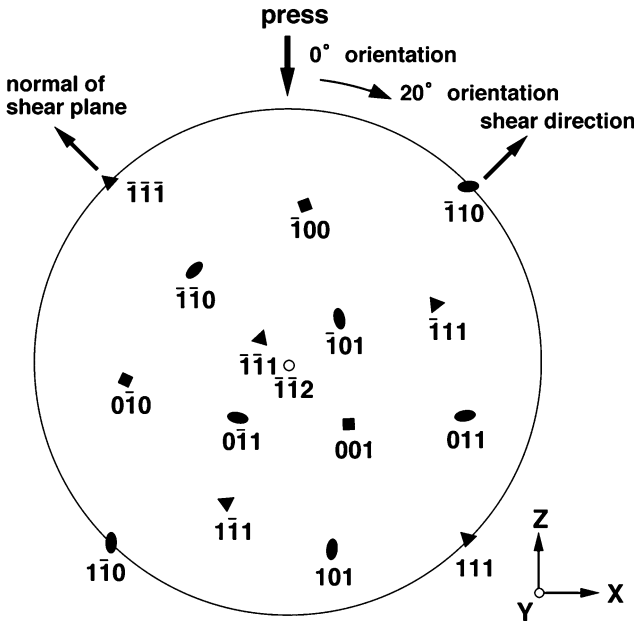

Fig. 3 The stereographic projection illustrating the relationship between the crystal orientation and the vertical pressing direction: information is given for the 0° orientation and the 20° orientation is rotated in a clockwise sense by 20°

Table 1 Calculations of shear factors for the 0° orientation

Slip plane	Slip direction	At entrance to shear zone		On 45° shear plane		At exit from shear zone	
		Shear factor	Order of shear factor	Shear factor	Order of shear factor	Shear factor	Order of shear factor
$\bar{1}\bar{1}\bar{1}$	$\bar{1}10$	0.93	(1)	1.00	(1)	0.93	(1)
	$\bar{1}10$	0.47	(2)	0.50	(2)	0.47	(2)
	$0\bar{1}1$	0.47	(2)	0.50	(2)	0.47	(2)
$\bar{1}11$	$\bar{1}\bar{1}0$	0.02	(12)	0.00	(11)	0.11	(8)
	$0\bar{1}1$	0.05	(10)	0.17	(5)	0.26	(6)
	101	0.03	(11)	0.17	(5)	0.37	(4)
$1\bar{1}1$	$\bar{1}\bar{1}1$	0.11	(8)	0.00	(11)	0.02	(12)
	$\bar{1}0\bar{1}$	0.26	(6)	0.17	(5)	0.05	(10)
	011	0.37	(4)	0.17	(5)	0.03	(11)
$\bar{1}\bar{1}1$	$\bar{1}10$	0.31	(5)	0.33	(4)	0.31	(5)
	011	0.22	(7)	0.17	(5)	0.09	(9)
	101	0.09	(9)	0.17	(5)	0.22	(7)

Table 2 Calculations of shear factors for the 20° orientation

Slip plane	Slip direction	At entrance to shear zone		On 45° shear plane		At exit from shear zone	
		Shear factor	Order of shear factor	Shear factor	Order of shear factor	Shear factor	Order of shear factor
$\bar{1}\bar{1}\bar{1}$	$\bar{1}10$	0.99	(1)	0.88	(1)	0.67	(1)
	$\bar{1}10$	0.50	(2)	0.44	(2)	0.33	(4)
	$0\bar{1}1$	0.50	(2)	0.44	(2)	0.33	(4)
$\bar{1}11$	$\bar{1}\bar{1}0$	0.03	(11)	0.16	(8)	0.35	(3)
	$0\bar{1}1$	0.20	(6)	0.28	(6)	0.30	(6)
	101	0.24	(5)	0.44	(2)	0.66	(2)
$1\bar{1}1$	$\bar{1}\bar{1}1$	0.02	(12)	0.01	(10)	0.09	(9)
	$\bar{1}0\bar{1}$	0.13	(9)	0.00	(12)	0.08	(10)
	011	0.11	(10)	0.01	(11)	0.01	(12)
$\bar{1}\bar{1}1$	$\bar{1}10$	0.33	(4)	0.29	(5)	0.23	(8)
	011	0.14	(8)	0.05	(9)	0.02	(11)
	101	0.19	(7)	0.23	(7)	0.24	(7)

entrance to the shear zone due to the arc of curvature, on the 45° shear plane as depicted in Fig. 1 and at the point of exit from the shear zone, respectively. Finally, the fourth, sixth and eighth columns rank the magnitudes of these shear factors for each location. It follows from these calculations that slip occurs preferentially on the $(\bar{1}\bar{1}\bar{1})[\bar{1}10]$ system under all conditions as the crystal in the 0° orientation passes through the shear zone and the secondary slip systems are $(\bar{1}\bar{1}\bar{1})[\bar{1}01]$ and $(\bar{1}\bar{1}\bar{1})[0\bar{1}1]$. The results are similar for the primary slip system in the crystal having the 20° orientation but the $(\bar{1}\bar{1}\bar{1})[\bar{1}01]$, $(\bar{1}\bar{1}\bar{1})[0\bar{1}1]$ and $(\bar{1}11)[101]$ systems have equal shear factors when the crystal reaches the 45° shear plane and at the point of exit from the die the $(\bar{1}11)[101]$ system has a shear factor which is larger, by a factor of two, than the $(\bar{1}\bar{1}\bar{1})[\bar{1}01]$ and $(\bar{1}\bar{1}\bar{1})[0\bar{1}1]$ slip systems and the $(\bar{1}11)[\bar{1}\bar{1}0]$ is then the third most important slip system.

Experimental results

It is convenient to consider separately the results obtained for the two different crystal orientations.

Single crystal in 0° orientation

Figure 4 shows several OM images for the single crystal having the 0° orientation: all images were recorded on the *Y* plane, the crystal is shown after removal from the die at the bottom of Fig. 4, the positions labeled 1 to 4 selected for detailed examination are documented in the image shown on the left and the individual images at points 1 to 4 are shown in the upper right. Several observations can be reached by careful inspection of these images. At point 1 near the upper face of the billet there are faint striations lying parallel to the *X* direction. At point 2 there are broad

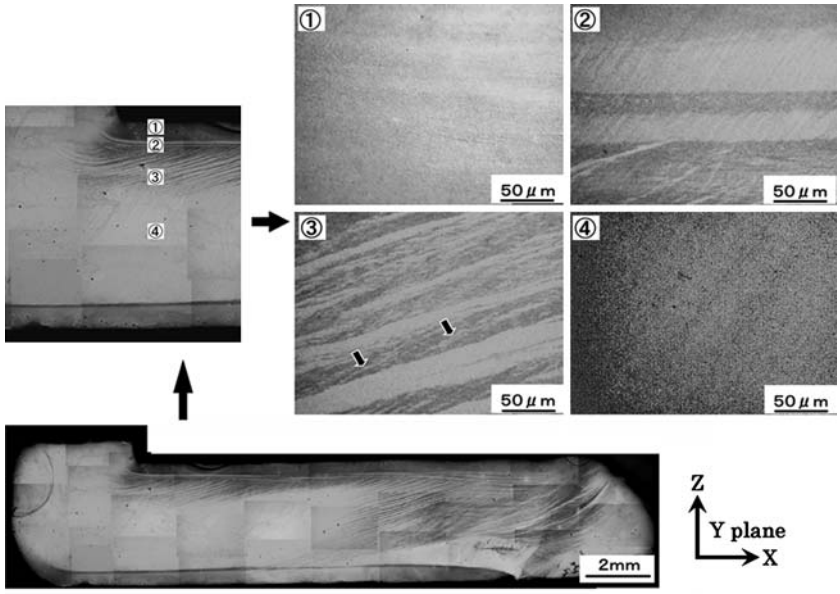

Fig. 4 The 0° orientation sample after pressing for one pass: the sample is shown at the bottom, four separate points are labeled on the left and the optical images at these four points are shown on the right

striations with widths of ~30–50 μm lying parallel to the *X* direction and fine striations inclined at an angle of 60° to the *X* axis. At point 3 there are broad striations with widths of ~5–30 μm inclined at angles in the range of 15°–20° to the *X* direction and, in addition, there are fine striations inclined at 25° to the *X* axis: examples of these fine striations are marked with arrows in Fig. 4. At point 4 near the central line of the billet there are very fine striations inclined at 55° to the *X* direction, where these striations correspond to assemblies of slip traces for several slip systems. Figure 5 shows additional OM images recorded on the *X* plane at two different magnifications and revealing the presence of wavy striations lying essentially parallel to the *Y* direction.

The (111) pole figures and OIM images at points 3 and 4 are shown in Fig. 6 together with additional information for a point labeled 0 lying in the undeformed region of the billet at the point which has not yet entered the shearing zone. Thus, the color-coded image at point 0 is pink and, as expected and based on the crystallographic triangle shown in Fig. 6, this corresponds to a ⟨112⟩ direction which is consistent with the (111) pole figure and represents the initial orientation of the crystal. In the vicinity of point 3, the color-coded OIM image shows alternating striations of pink and light blue inclined at angles in the range of 15°–20° from the *X* direction, where this corresponds to the OM image at point 3 in Fig. 4. It is also apparent from the (111) pole figure for point 3 that the initial orientation is present together with an orientation rotated by 60° in a counter-clockwise direction from the initial orientation. This microstructure with duplex orientations is equivalent to the conventional B_2-type texture which was observed in earlier experiments using an aluminum single crystal tested with an initial 0° orientation [10]. Finally, the OIM image for position 4 shows a structure which is reasonably similar to the initial orientation and this similarity is confirmed by the (111) pole figure.

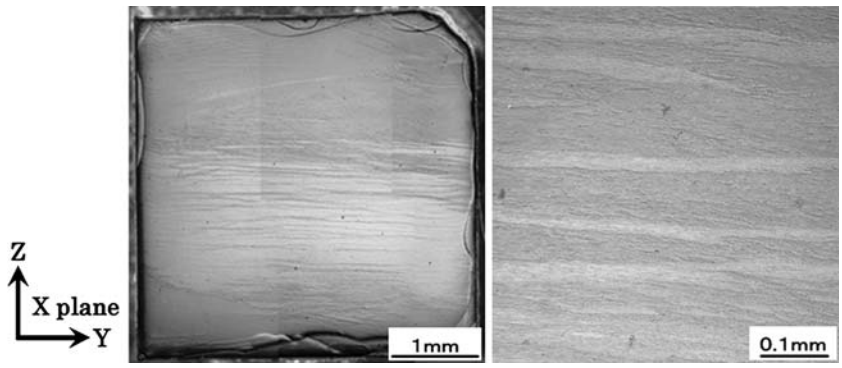

Fig. 5 Optical images at two different magnifications for the 0° orientation on the *X* transverse plane

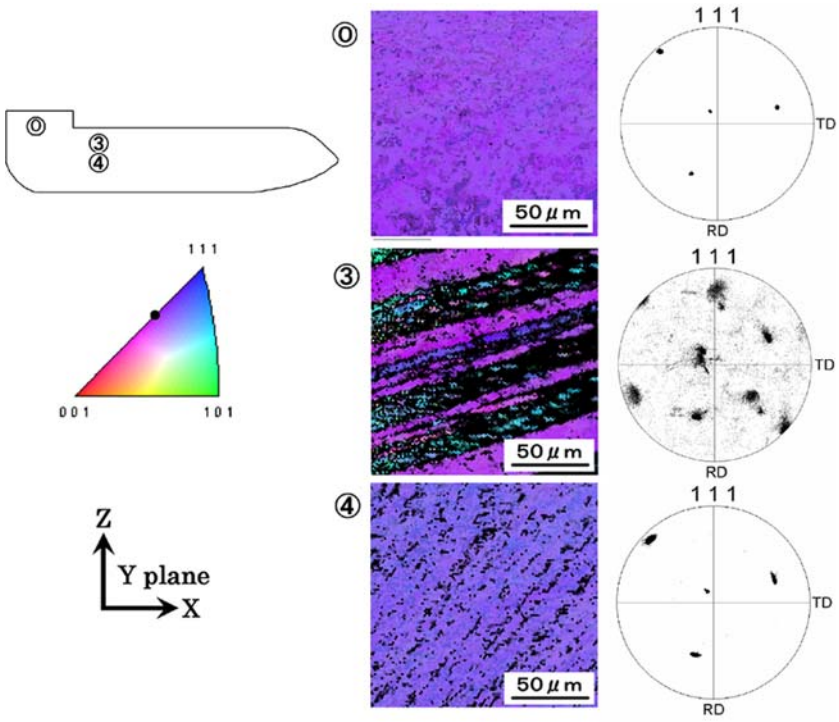

Fig. 6 Images taken using orientation imaging microscopy for the 0° orientation and the corresponding (111) pole figures for the positions labeled 0, 3 and 4: the colors relate to the crystallographic orientations shown in the stereographic triangle

Further information on the nature of the deformation may be obtained by examining the TEM photomicrograph shown in Fig. 7 where the TEM image was taken in the vicinity of point 3 in Figs 4 and 6 and the three selected area electron diffraction (SAED) patterns were recorded from areas having diameters of 6.15 μm within the two wide regions labeled A and C and the intermediate narrow region labeled B. Thus, it is apparent that the SAED patterns from regions A and C correspond to the initial orientation whereas the SAED pattern in the narrow region B shows the initial orientation and an orientation rotated by 60° about the *Y* axis in a counter-clockwise sense from the initial orientation. The presence of discrete spots in all of the SAED patterns with diffusing angles of <15° demonstrates the presence of boundaries having low angles of misorientation and this is consistent with the low strain imposed in a single pass. It is also apparent from the TEM photomicrograph that the boundaries between regions A and B and regions B and C are inclined at an angle of approximately 20° with the *X* axis. Furthermore, close inspection shows that the microstructures in regions A and C are similar and consist of arrays of elongated cells or subgrains inclined at an angle of approximately 45° with the *X* axis. Measurements showed the widths of these subgrain arrays, measured perpendicular to the long axes, were ~0.2 μm and the orientation of these long axes were parallel to the primary $(\bar{1}\bar{1}1)[\bar{1}10]$ slip system: this is illustrated by the schematic diagram on the lower left of Fig. 7. For comparison with the SAED pattern for the narrow region B, the diagram on the lower right of Fig. 7 depicts the effect of a counter-clockwise rotation by 60° and it is apparent that the slip traces in region B, although not clearly defined, are generally not consistent with slip on the primary $(\bar{1}\bar{1}1)[\bar{1}10]$ slip system.

Single crystal in 20° orientation

Figure 8 shows the OM images for the single crystal having the 20° orientation and two high magnification images taken from the points labeled 1 and 2. For this orientation, the low magnification image shows an essentially uniform deformation throughout the width of the billet. This uniformity is confirmed in the images at the higher magnification where both images reveal fine striations lying in the angular range of 40°–60° to the *X* direction. The corresponding images on the *X* plane are shown in Fig. 9 at low and high magnifications and again there is a uniformity across the section with prominent striations lying approximately parallel to the *Y* axis.

The OIM images and (111) pole figures are shown in Fig. 10 with separate images for the same positions labeled 1 and 2 and for an additional position 0 lying in the initial unpressed section of the billet. For position 0 before the shearing zone, the color-coded image is pink showing a ⟨112⟩ direction and the (111) pole figure is

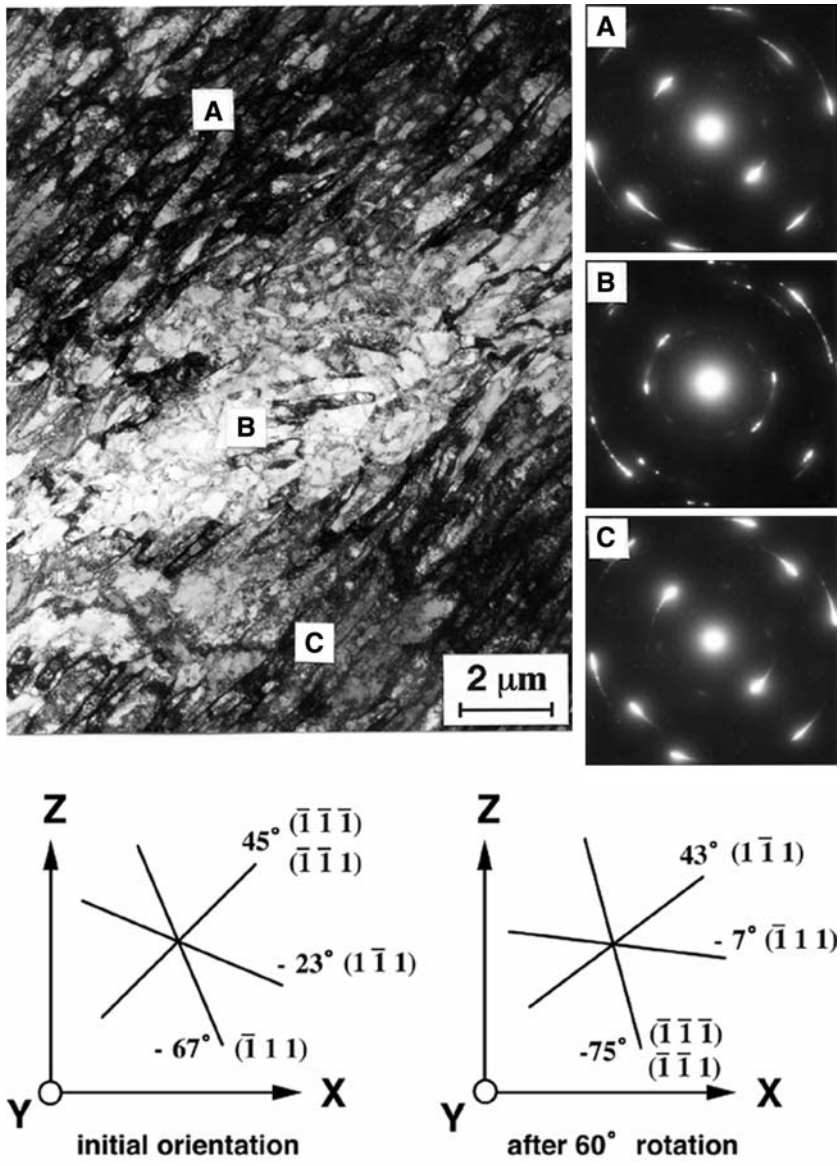

Fig. 7 A TEM photomicrograph for the 0° orientation showing the presence of distinct regions and the associated SAED patterns for these regions: the lower illustrations depict the effect of a 60° rotation from the initial orientation

similar to the initial orientation. The color-coded images in Fig. 10 show there are striations inclined at about 45° to the *X* direction at positions 1 and 2 and both of the (111) pole figures show an orientation rotated by 20° about the *Y* axis in a counter-clockwise direction from the initial orientation.

Careful inspection by TEM revealed the presence of two different structures within the deformed part of the billet. These two structures are illustrated in Fig. 11a, b where the SAED patterns were taken from areas within each structure having diameters of 12.3 μm and the lower schematic illustration shows the initial orientation on the left and the effect of a 20° rotation on the right. In Fig. 11a there is an array of cells or subgrains oriented at 45° to the *X* direction but in Fig. 11b there are two sets of intersecting subgrain boundaries oriented with respect to the *X* axis at 45° and –20°, respectively. For both photomicrographs, the widths of the subgrain arrays are ~0.2 μm. Furthermore, both of the SAED patterns in Fig. 11 reveal a rotation by 20° about the *Y* axis in a counter-clockwise sense from the initial orientation. In both regions the TEM images show the long axes of the subgrain arrays lie at 45° to the *X* axis and they are parallel to the slip traces of the primary $(\bar{1}\bar{1}\bar{1})[\bar{1}10]$ slip system after a rotation by 20°. In Fig. 11b, the long axes of the subgrain arrays lie at minus 20° to the *X* axis and they are parallel to the slip traces for slip on the $(1\bar{1}1)$ plane after rotation by 20° in a counter-clockwise direction despite the fact that, as shown in Table 2, the shear

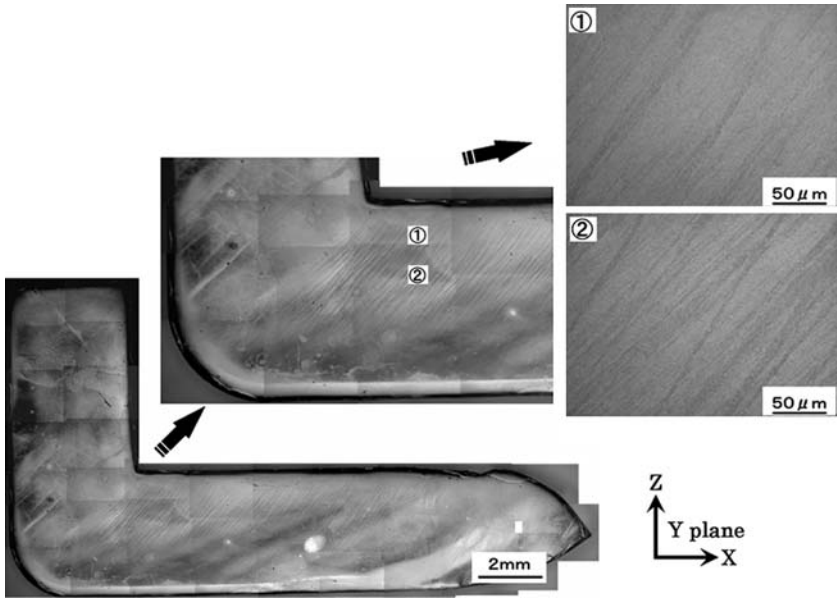

Fig. 8 The 20° orientation sample after pressing for one pass: the sample is shown at the bottom, two separate points are labeled in the center and the optical images at these two points are shown on the right

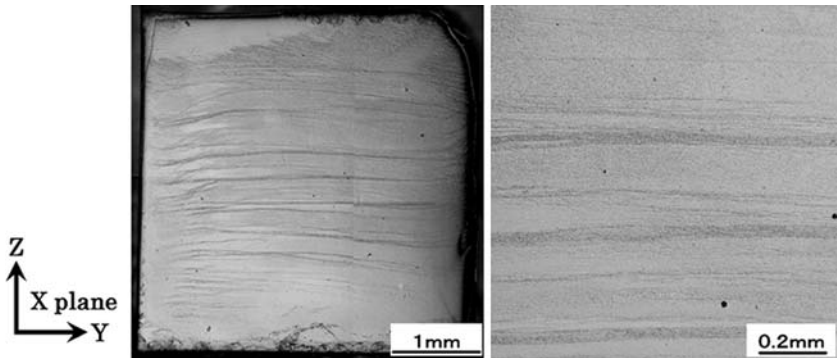

Fig. 9 Optical images at two different magnifications for the 20° orientation on the *X* transverse plane

factors for slip on the $(1\bar{1}1)$ plane are very small. This observation suggests that the primary slip system is activated on entry into the shearing zone but the passage of the crystal through the shearing zone leads to a rotation in a counter-clockwise sense about the *Y* axis [10, 14] so that slip becomes progressively easier on the $(1\bar{1}1)$ plane.

Discussion

General observations

These results demonstrate that the initial orientation of a single crystal plays a critical role in determining the deformation behavior when the crystal passes through an ECAP die. For the two orientations of copper single crystals tested in these experiments, several conclusions may be drawn.

First, for the crystal in the 0° orientation the OM images and the (111) pole figures demonstrate the presence of two crystallographic orientations after ECAP corresponding to the initial orientation and to an orientation rotated by 60° about the *Y* axis in a counter-clockwise sense from the initial orientation. For regions having the initial orientation, there are arrays of elongated cells or subgrains lying parallel to the slip trace of the primary $(\bar{1}\bar{1}\bar{1})[\bar{1}10]$ slip system whereas for the regions where the orientation has rotated by 60° the slip traces no longer correspond to the primary slip system. This leads to two separate orientations and a B_2-type texture within the deformed section of the billet. A similar result was reported earlier for an aluminum single crystal tested with a 0° orientation [10].

Second, for the crystal in the 20° orientation the deformation characteristics are significantly more simple than for the 0° orientation. Careful inspection

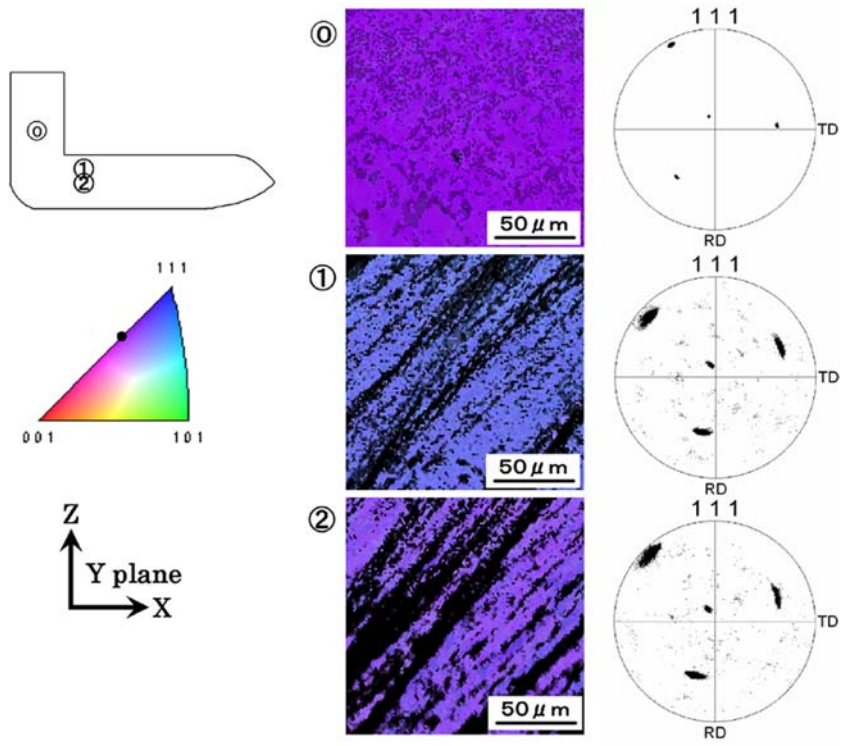

Fig. 10 Images taken using orientation imaging microscopy for the 20° orientation and the corresponding (111) pole figures for the positions labeled 0, 1 and 2: the colors relate to the crystallographic orientations shown in the stereographic triangle

revealed evidence for only a single crystallographic orientation which is rotated by 20° about the *Y* axis in a counter-clockwise sense from the initial orientation. However, two different slip traces were visible and these are consistent with the primary $(\bar{1}\bar{1}\bar{1})[\bar{1}10]$ slip system and, despite estimates of relatively low shear factors, with a slip system operating on the $(1\bar{1}1)$ plane.

Third, the rotation in a counter-clockwise sense is a natural consequence of making observations on the Y plane such that the entrance channel is at the upper left and the exit channel is at the lower right. As the billet moves through the die, it rotates on the *Y* plane in a counter-clockwise sense during passage through the shearing zone [14]. Furthermore, this rotation is an inevitable feature of the pressing operation because, even if there is no angle marking the outer arc of curvature where the two parts of the channel intersect so that $\Psi = 0°$, there will be a corner gap or dead zone at the outer corner which will lead to a similar effect [15–19].

Comparison with ECAP of aluminum and copper single crystals

Several earlier reports documented the processing of aluminum single crystals by ECAP using initial orientations of (a) 0° [10], (b) 20° [11] and (c) –20° [12]. It is instructive to make a direct comparison between the behavior of aluminum and copper.

In the present experiments on Cu single crystals, the first pass through the shearing zone leads to arrays of elongated cells or subgrains having measured average widths, for both initial orientations, of ~0.2 μm. In aluminum single crystals, there were similar arrays of elongated subgrains but the measured average width after a single pass was ~1.3 μm. It was shown for aluminum that this width is consistent with experimental data for polycrystalline aluminum where the average equilibrium grain size produced by ECAP through a number of passes at room temperature is also ~1.3 μm [20, 21]. Thus, it was concluded for aluminum that the ultimate equilibrium grain size is dictated by the subgrain width on the first passage through the die and the same conclusion is now reached from the present experiments on copper. It is well established in practice that the equilibrium grain size attained in ECAP decreases with decreasing rates of recovery and therefore with decreasing values of the stacking-fault energy [22] such that in pure Cu the equilibrium grain size formed in ECAP processing was measured earlier as ~0.27 μm [23]. This latter value is very similar to the widths of the subgrains measured in these experiments in the Cu single crystals.

A second feature of the pressing of aluminum single crystals is that the long axes of the arrays of subgrains

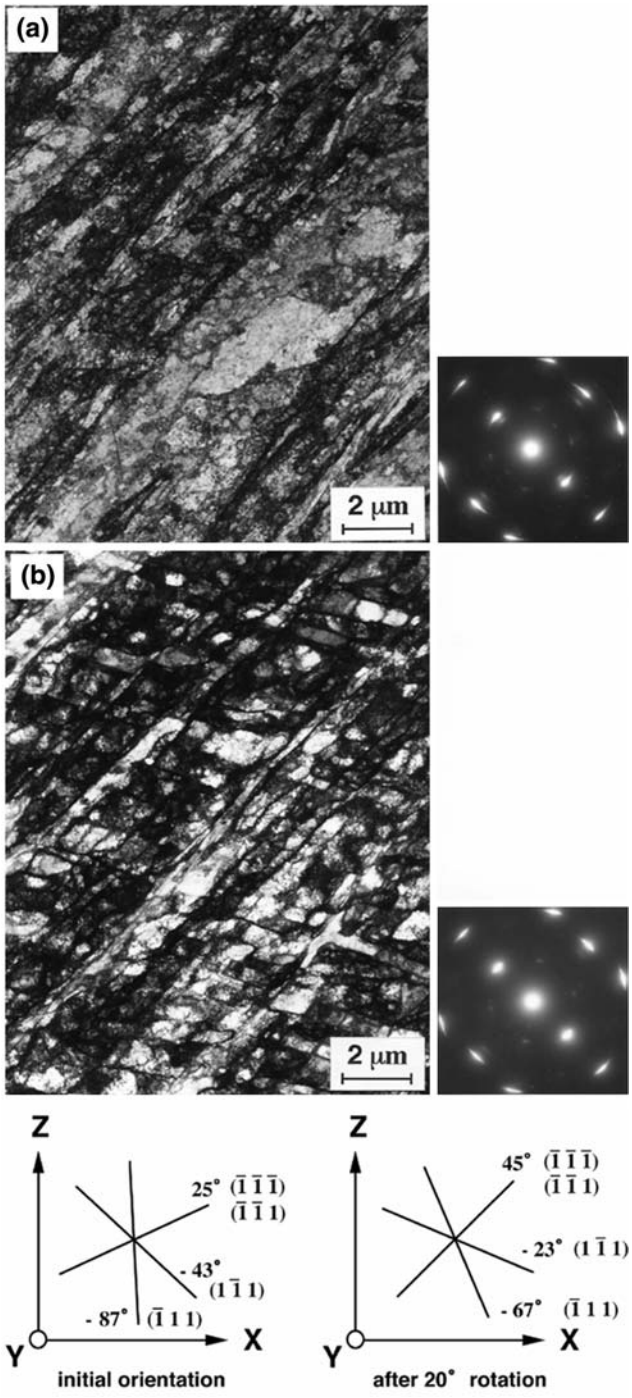

Fig. 11 Photomicrographs taken using TEM for the 20° orientation showing the presence of two distinct regions labeled (**a**) and (**b**) and the associated SAED patterns for these regions: the lower illustrations depict the effect of a 20° rotation from the initial orientation

generally lie parallel to the primary slip system [12]. This is also supported by the experiments on copper single crystals where, at least in major parts of the crystals, the subgrain arrays are also similarly oriented.

There is an additional similarity because a B_2-type texture was formed in an aluminum single crystal with an initial 0° orientation and a similar texture was formed also in copper with the same initial orientation. Furthermore, both the aluminum and copper single crystals exhibited slip predominately on a single system when testing in the initial 20° orientation but there is an important difference because in aluminum there was a counter-clockwise rotation by 40° whereas in copper there was a counter-clockwise rotation by 20° as shown by the (111) pole figures for positions 1 and 2 in Fig. 10. This difference is probably due to the different values for the strain hardening rates in these two crystals. It may be significant to note also that the magnitude of the corner gap at the outer arc of curvature in the ECAP die appears to depend directly upon the strain hardening behavior of the billet [15] and it is apparent that the presence of a corner gap will necessarily influence the angle of rotation within the crystal.

Finally, there are some limited data reported for the processing of copper single crystals by ECAP [24, 25] but it is difficult to make a direct comparison with the present experiments. This difficulty arises because the emphasis was placed in this earlier work on the development of shear bands [24] and the results reported from the pressing of several billets with different initial orientations divide the crystals into three distinct macroscopic categories that are not easily interpreted in terms of the present analysis [25].

Summary and conclusions

1. Two single crystals of high-purity copper were processed through one pass in equal-channel angular pressing (ECAP) at room temperature using a die with an internal channel angle of 90° and with the *Y* direction in the ECAP die coincident with the ⟨112⟩ direction in the crystals. The two crystals were in different orientations: (i) the 0° orientation with the (111) slip plane parallel to the theoretical shear plane and the [110] slip direction parallel to the direction of shear and (ii) the 20° orientation where the crystal was rotated by 20° in a clockwise sense about the ⟨112⟩ direction.
2. For both orientations, a single pass leads to the formation of an elongated array of cells or subgrains where the boundaries have low angles of misorientation and the long axes of the arrays are aligned parallel to the primary $(\bar{1}\bar{1}1)[\bar{1}10]$ slip

system. This is consistent with results obtained earlier using aluminum single crystals.

3. For both orientations, the width of the subgrain array was measured as ~0.2 μm which is similar to the equilibrium grain size reported in polycrystalline Cu after processing by ECAP. A similar result was reported earlier for aluminum single crystals except that the subgrain width and the equilibrium grain size are significantly larger in aluminum (~1.3 μm). The lower values in Cu are attributed to the low stacking-fault energy and the low rate of recovery.
4. As in pure aluminum, a copper single crystal in a 0° orientation gave two separate orientations and a B_2-type texture after a single pass. For the copper single crystal in the 20° orientation, the deformed sample contained a single crystallographic orientation which was rotated by 20° in a counterclockwise sense from the initial orientation.

Acknowledgements This work was supported in part by the Light Metals Educational Foundation of Japan and in part by the National Science Foundation of the United States under Grant No. DMR-0243331.

References

1. Valiev RZ, Islamgaliev RK, Alexandrov IV (2000) Prog Mater Sci 45:102
2. Lowe TC, Zhu YT (2003) Adv Eng Mater 5:373
3. Segal VM (1995) Mater Sci Eng A197:157
4. Segal VM (2004) Mater Sci Eng A386:269
5. Horita Z, Fujinami T, Langdon TG (2001) Mater Sci Eng A318:34
6. Semiatin SL, DeLo DP (2000) Mater Design 21:311
7. Alexandrov IV, Raab GI, Shestakova LO, Valiev RZ, Dowding RJ (2000) In: Greenfield MS, Oakes JJ (eds) Tungsten, hard metals and refractory alloys 5. Metal Powder Industries Federation, Princeton NJ, pp 27–45
8. Furukawa M, Iwahashi Y, Horita Z, Nemoto M, Langdon TG (1998) Mater Sci Eng A257:328
9. Furukawa M, Horita Z, Langdon TG (2002) Mater Sci Eng A332:97
10. Fukuda Y, Oh-ishi K, Furukawa M, Horita Z, Langdon TG (2004) Acta Mater 52:1387
11. Furukawa M, Kawasaki Y, Miyahara Y, Horita Z, Langdon TG (2005) Mater Sci Eng A410–411:194
12. Fukuda Y, Oh-ishi K, Furukawa M, Horita Z, Langdon TG (2006) Mater Sci Eng A420:79
13. Iwahashi Y, Wang J, Horita Z, Nemoto M, Langdon TG (1996) Scr Mater 35:143
14. Yoshida Y, Cisar L, Kamado S, Koike J, Kojima Y (2003) Mater Sci Forum 419–422:533
15. Kim HS, Seo MH, Hong SI (2000) Mater Sci Eng A291:86
16. Kim HS (2001) Mater Sci Eng A315:122
17. Park JW, Suh JY (2001) Metall Mater Trans A 32A:3007
18. Kim HS (2002) J Mater Res 17:172
19. Semiatin SL, DeLo DP, Park JW (2002) J Mater Proc Tech 122:255
20. Iwahashi Y, Horita Z, Nemoto M, Langdon TG (1998) Acta Mater 46:3317
21. Terhune SD, Swisher DL, Oh-ishi K, Horita Z, Langdon TG, McNelley TR (2003) Metall Mater Trans A 33A:2173
22. Iwahashi Y, Horita Z, Nemoto M, Langdon TG (1998) Metall Mater Trans A 29A:2503
23. Komura S, Horita Z, Nemoto M, Langdon TG (1999) J Mater Res 14:4044
24. Miyamoto H, Erb U, Koyama T, Mimaki T, Vinogradov A, Hashimoto S (2004) Philos Magn Lett 84:235
25. Miyamoto H, Fushimi J, Mimaki T, Vinogradov A, Hashimoto S (2005) Mater Sci Eng A405:221